Convective Instability and Mass Transport of Diffusion Layers in a Hele-Shaw Geometry

Scott Backhaus,[1,*] Konstantin Turitsyn,[2,3] and R. E. Ecke[3]

[1]*MPA-CMMS, Los Alamos National Laboratory, Los Alamos, New Mexico 87545, USA*
[2]*Theoretical Division, Los Alamos National Laboratory, Los Alamos, New Mexico 87545, USA*
[3]*Center for Nonlinear Studies, Los Alamos National Laboratory, Los Alamos, New Mexico 87545, USA*

We consider experimentally the instability and mass transport of flow in a Hele-Shaw geometry. In an initially stable configuration, a lighter fluid (water) is located over a heavier fluid (propylene glycol). The fluids mix via diffusion with some regions of the resulting mixture being heavier than either pure fluid. Density-driven convection occurs with downward penetrating dense fingers that transport mass much more effectively than diffusion alone. We investigate the initial instability and the quasisteady state. The convective time and velocity scales, finger width, wave number selection, and normalized mass transport are determined for $6000 < \mathrm{Ra} < 90\,000$. The results have important implications for determining the time scales and rates of dissolution trapping of carbon dioxide in brine aquifers proposed as possible geologic repositories for sequestering carbon dioxide.

PACS numbers: 47.20.Bp, 47.15.gp, 47.56.+r

Convective processes that transport heat and mass are critical to many natural phenomena in the atmosphere, oceans, and planetary and stellar interiors [1]. Another important example of current scientific and technological interest is the convective mixing of supercritical CO_2 sequestered in a brine-saturated porous medium [2], i.e., a deep saline aquifer. When injected into such aquifers, the low density CO_2 rises to the top of the aquifer where it is contained by cap rock formations. As a pure phase, the buoyancy of the supercritical CO_2 may drive it back to the surface, defeating attempts to sequester it. Diffusion into the underlying brine results in a denser mixture eliminating buoyancy, but this process is very slow and the pure phase of supercritical CO_2 would remain mostly intact for long times ($\approx 10\,000$ yr) unless other processes occur.

One scenario for enhanced dissolution of the CO_2 is gravitationally driven convection which relies on the increased density of CO_2-brine mixtures [2]. However, similar to thermal layers [3], the diffusion layer must thicken enough to become unstable. Analytical and numerical calculations have been performed [4–9] to predict the instability incubation time and subsequent mass transport in CO_2-brine systems. However, the difficulties in realizing a laboratory experiment for the purposes of testing the scenario are considerable, e.g., establishing the stable initial conditions assumed by calculations and the high pressure (≈ 100 bar) required in direct experiments with supercritical CO_2. Instead, we have developed an atmospheric-pressure analog fluid system that mimics many features of the CO_2-brine system. It consists of water located vertically above propylene glycol (PPG) in a Hele-Shaw cell where water replaces the CO_2 and PPG replaces the brine. In this cell, we can create relatively unperturbed initial conditions such that the instability occurs uniformly across the cell width. We measure the temporal evolution

using optical shadowgraph and determine the wave number selection, the time and velocity scales, the finger width, and the mass transport rate. Our results establish the basic description of diffusively driven convective instability in such systems.

The experimental apparatus in Fig. 1 is a vertically oriented Hele-Shaw cell with two 1.2-cm-thick polycarbonate sheets separated by steel shims of thickness b. The flow in the narrow gap b obeys Darcy's law with an isotropic permeability $K = b^2/12$ and a porosity of unity. We vary b from 0.25 to 0.48 mm giving values of K in the range 5000–20 000 Darcy (i.e., $0.54 \times 10^{-4} \leq K \leq 1.94 \times 10^{-4}$ cm^2). The lateral dimension of the flow region is 7.6 cm, and the initial depth of the bottom fluid H ranges from 1.25 to 5 cm. Water ($\rho_w = 1.000$ g/cc) is lighter than PPG ($\rho_{\mathrm{PPG}} = 1.035$ g/cc [10]) and is initially above the PPG. Water-PPG mixtures with a water concentration c_w between 0 and $\approx 50\%$ have $\rho \geq \rho_{\mathrm{PPG}}$. After a period of diffusive growth, the fluid interface may become gravitationally unstable, similar to the proposed instability when supercritical CO_2 dissolves into brine. There are, however, some important differences between the two fluid systems. Water and PPG are fully miscible, whereas CO_2 is partially miscible in brine with a low saturation concentration so that the transport properties of the CO_2-brine system do not depend strongly on the CO_2 concentration. In contrast, the viscosity and mass diffusivity of the water-PPG system are highly dependent on water concentration c_w. However, the important convective dynamics occurs in the downward moving fingers and the dense diffusive layer that feeds them [see Fig. 1(d)], and until they reach the bottom of the cell, the fingers do not significantly mix with the pure PPG maintaining a relatively constant water concentration. Therefore, when computing experimental parameters or making comparisons to calculations or
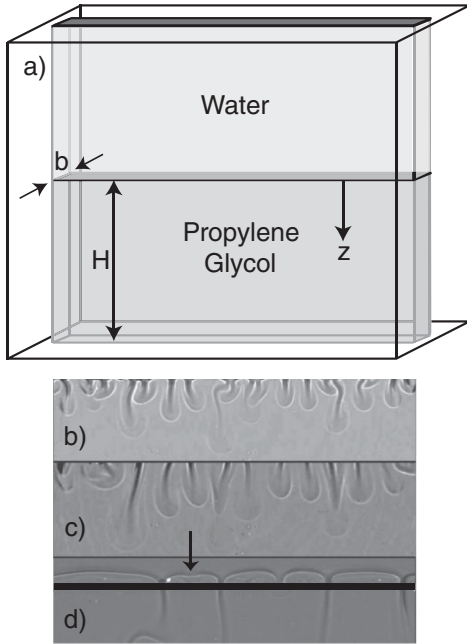
FIG. 1. (a) Schematic illustration of the Hele-Shaw cell where gap width b, PPG reservoir height H, and vertical coordinate z are indicated. A thin metal shim separating the two fluids is withdrawn horizontally to begin an experimental run. Images at three intermediate times t^* are shown for a run with $K = 1.9 \times 10^{-4}$ cm^2 and Ra = 87 000: (b) $t^* = 2.0$, (c) $t^* = 3.0$, (d) $t^* = 10.0$. Only a portion of the vertical extent of the image is shown. As seen in (d), light scattering off of the metallic shims makes the precise location of the interface uncertain. The vertical arrow in (d) indicates the nucleation site of a new finger.

simulations, we use the transport properties of a $c_w = 0.3$ mixture, i.e., $\nu = 0.1$ cm^2/s [10] and $D = 1 \times 10^{-6}$ cm^2/s (estimated using data from [11]), which corresponds to the mixture of maximum density $\rho = 1.044$ g/cc or the maximum density difference of $\Delta\rho = 0.009$ g/cc relative to the underlying PPG. Near $c_w = 0.3$, both ν and D are relatively constant, reducing any effects of their variability. We note that our experimental setup and fluid system are somewhat similar to those used in [12,13]. However, the experiments in [12] appeared to show finite cell-size effects, and our Rayleigh numbers (defined below) are a factor of 10 lower than in [13]. Also, we vary the Rayleigh number (defined below) using K and H as opposed to K and $\Delta\rho$ [13].

The upper and lower sections of the Hele-Shaw cell are separated by a system of shims of maximum thickness 0.01 cm. The upper and lower reservoirs are filled with pure water and pure PPG, respectively. A 0.0076-cm-thick "shutter shim" is removed horizontally from between the two fluids leaving behind the 0.01-cm-thick "frame shim" to ensure a liquid-tight seal. The small fluid perturbations induced did not appear to influence the flow for measurements presented here. The 0.01-cm-thick frame shim leaves a horizontal gap between the upper and lower cells

which our cell filling method ensures is filled by water after the shim removal [14].

The development of the flow and mixture concentration is visualized by optical shadowgraph over an area $L = 3.0$ cm wide (1280 pixels) and 2.4 cm high (1024 pixels). Each run consists of approximately 2000 frames with total run times between 2.5 and 10 h. Figures 1(b)–1(d) show the evolution of a typical experimental run at various times after initiation. Initially, the PPG preferentially diffuses into the water owing to an asymmetric dependence of $D(C)$ [11]. The dense diffusion layer thickens, buoyancy overcomes lateral diffusion, and instability occurs as small perturbations in the interface grow into downward moving fingers.

Nondimensional scalings and solution techniques for the conservation of momentum, mass, and concentration are described in detail elsewhere [4–9]. Here, we discuss the dimensionless parameters and a few details relevant to our experiment. Under the conditions of the experiment, the fluids and their mixture are incompressible [15,16]. The maximum Reynolds number (based on b) is less than 10^{-3}, justifying the use of a two-dimensional Darcy's law. Near the finger tips and the finger cores the Peclet number can approach 50, and the advection-diffusion equation may be modified by Taylor dispersion [17] with the effective diffusion coefficient 15 times larger than molecular diffusion.

Neglecting the impact of Pe within the finger cores, the Rayleigh number Ra $= \Delta\rho g K H/\rho\nu D$ governs the flow [4–9]. Here, g is the acceleration due to gravity and all fluid properties are evaluated at $c_w = 0.3$. The vertical convective motion of a blob of fluid with $c_w = 0.3$ is a balance between buoyancy and viscous drag, i.e., $v_c = \Delta\rho g K/\rho\nu$. At v_c, this blob falls the entire depth H in Fig. 1 in time $t_c = H/v_c = H/(\Delta\rho g K/\rho\nu)$. We define $t^* = t/t_c$. Comparative time and velocity scales are the diffusion time $t_d = H^2/D$, i.e., the approximate time to establish a diffusion gradient over H, and the diffusion velocity $v_d = D/H$. We see that Ra $= t_d/t_c = v_c/v_d$ describes the importance of convection relative to diffusion over the vertical distance H.

First, we consider the finger dynamics from instability onset to steady state [i.e., Figs. 1(b)–1(d)]. At onset, there are many closely spaced fingers, and this pattern coarsens via two mechanisms. When short compared to their width, some fingers stagnate and disappear, which we interpret as longer dominant fingers preferentially draining dense mixture from the diffusion interface. At all times, fingers move laterally along the interface, collide, and merge, resulting in the coarse pattern of Fig. 1(d). Figure 2(a) characterizes the coarsening process showing the inverse of the scaled average finger spacing δ/λ versus the scaled depth z/δ of the longest finger. Here, δ is the measured finger width and λ is the average finger-to-finger spacing. Near the instability onset at $z/\delta \approx 1$, δ/λ ranges between 0.22 and 0.27, consistent with the onset value of $\delta/\lambda \approx 0.27$ computed from the results in Sec. 4 of [6]. (Determining the onset λ is relatively simple; however, the limitations of our imaging
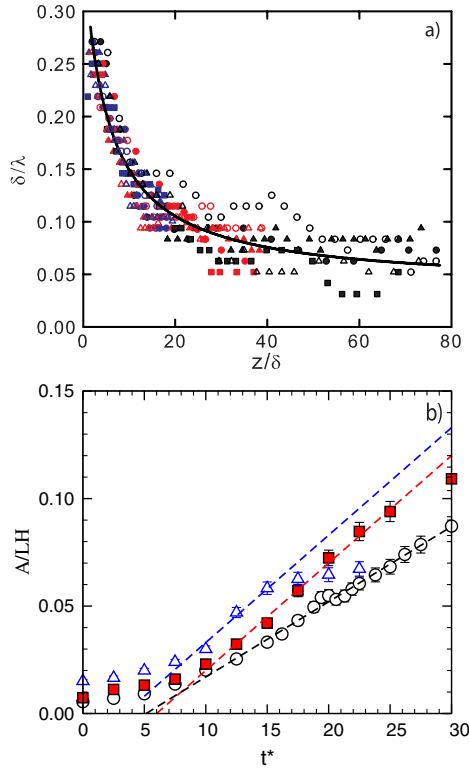
FIG. 2 (color online). (a) δ/λ vs z/δ. Different values of H are 1.27 cm [dark gray (blue)], 2.54 cm [light gray (red)], and 5.08 cm (black). The different symbols indicate different values of K. Over the range of the experiments, δ is roughly the same for all runs with an average value of $\delta = 0.065$ cm. The solid line is the best fit of the form $\delta/\lambda = (1.90 + 0.038z/\delta)/(5.30 + z/\delta)$. (b) Area of water consumed $A/(LH)$ vs t^* for several data sets with $K = 0.77 \times 10^{-4}$ cm^2 and Ra = 8700 (open triangles), Ra = 17 400 (solid squares), and Ra = 34 800 (open circles). The small offset in the initial A/LH is due to the uncertainty in the location of the initial fluid-fluid interface as described in the caption of Fig. 1.

system prohibit us from determining the onset time.) For larger z/δ, δ/λ decreases and appears to asymptotically approach $\delta/\lambda \approx 0.04$. We expect this behavior for two reasons. First, if $\delta/\lambda \to 0$, then the water flux per unit interface length would tend to zero for large z or H, which is unphysical. Second, the coarsening is eventually balanced by the nucleation of new fingers as the diffusion interface between two now distant fingers thickens and becomes unstable [see Fig. 1(d)]. For large H, this instability should be governed by local processes independent of H. After the longest finger extends to H, we observe some fluctuations in δ/λ, but the time average is close to the δ/λ near $z/\delta = H/\delta$ in Fig. 2(a). We conclude that interactions of the fingers with the bottom of the cell do not affect the pattern, and δ is an appropriate length scale for coarsening as opposed to H.

Understanding the convective and mixing processes is important for assessing its effectiveness to securely sequester CO$_2$ in brine reservoirs. The amount of water mixed is determined from the area A between the initial
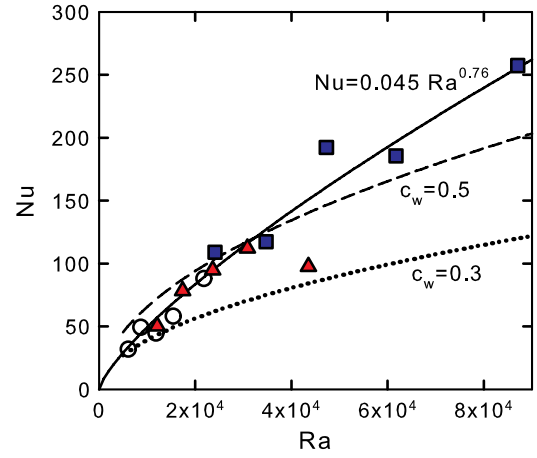

FIG. 3 (color online). Nu vs Ra. Different values of H are 1.27 cm (open circles), 2.54 cm (filled triangles), and 5.08 cm (filled squares). The solid line is the best power-law fit of the form Nu = 0.045Ra$^{0.76}$. The dashed and dotted lines are Nu computed from the simple mass flux model described in the text using the δ/λ fit in Fig. 2(a) for two different values of water concentration in the core of the descending fingers.

interface and the middle of the subsequent diffusive interface [as in Fig. 1(d)] [18]. Figure 2(b) shows A/LH vs t^* for several runs with the same K but different H. After an initial slow increase [14], A/LH increases linearly with t^* indicating a steady mass transfer rate. In runs with small H (e.g., the Ra = 8700 data), $A(t^*)/LH$ saturates as convection slows when the mixture density in the lower cell increases.

The Nusselt number Nu = $\dot{m}/\rho(D/H)bL$ is the actual mass flux normalized by the diffusive mass flux over cell depth H. Rewriting, Nu = Ra $d(A/LH)/dt^*$; i.e., Nu is simply Ra times the slopes from Fig. 3. Nu is plotted versus Ra in Fig. 3. A power-law fit shows Nu = (0.045 ± 0.025)Ra$^{0.76\pm0.06}$, similar to results from numerical simulations of thermal convection in three-dimensional porous media [19] where Nu ≈ 0.017Ra$^{0.9}$ for $10^3 <$ Ra $< 10^4$. Comparing values at Ra = 10 000, we find Nu ≈ 49, and thermal convection simulations give Nu ≈ 67. Although the comparison with simulation is reasonable, we seek to go further by checking the internal consistency of the data in Figs. 2(a) and 3 and using these results to outline a new stability problem that should provide a prediction of Nu.

The water mass flux through the fingers into the lower cell is given by $\rho c_w n \delta v_f b$, where n is the number of fingers extending from the interface and v_f is the velocity of the fluid in the finger cores. Scaling this mass flux we find Nu/Ra = $c_w(\delta/\lambda)(v_f/v_c)$. To estimate v_f/v_c, we consider a set of equally spaced fingers and ignore small density differences except in buoyancy terms. Balancing the mass flux at a horizontal line cutting through the fingers requires $v_f\delta = (\lambda - \delta)v_b$, where v_b is the upward velocity of pure PPG between the fingers. Integrating the vertical component of Darcy's law around a closed rectangular contour with one vertical leg in a

finger and the other in the pure PPG, we find $v_f = v_c - (\nu_b/\nu_f)v_b$. Combining the previous results yields $v_f/v_c = [1 + (\nu_b/\nu_f)\delta/(\lambda - \delta)]^{-1}$, allowing us to express Nu/Ra (from above) as a function solely of δ/λ; i.e. Nu/Ra $= c_w(\delta/\lambda)/[1 + (\nu_b/\nu_f)(\delta/\lambda)/(1 - \delta/\lambda)] \equiv c_w F[\delta/\lambda]$ (ν_b/ν_f is fixed in this experiment). In the quasisteady state after the fingers reach $z = H$, we can instead interpret the fitted curve $\delta/\lambda = G[z/\delta]$ in Fig. 2(a) as $\delta/\lambda = G[H/\delta]$. However, $H/\delta = $ Nu so that $\delta/\lambda = G[$Nu$]$. Combining, we find Nu/Ra $= c_w F[G[$Nu$]]$, which is numerically inverted to find Nu versus Ra as shown in Fig. 3 for $c_w = 0.3$ and 0.5, i.e., c_w at maximum mixture density and the maximum c_w where the mixture density is still greater than ρ_{PPG}.

The rough agreement in Fig. 3 supports the validity of this simple model of mass transfer and the relationship between Nu and the δ/λ behavior in Fig. 2(a). However, a full understanding of the mass transfer must include a theoretical model of δ/λ. Here, we describe the relevant physical processes leaving detailed modeling for future work. The core of this model is a new stability calculation that predicts the distance between two established fingers at which the intervening diffusion layer becomes unstable to small perturbations. However, this layer is already experiencing significant flow and Taylor dispersion due to fluid drainage from the layer into the fingers. Dispersion will smooth out concentration perturbations driving nucleation to the symmetry point between the fingers [see Fig. 1(d)] where the flow stagnates. At this point, streamwise velocity gradients will stretch and spread a nascent finger. Both of these mechanisms behave like enhanced diffusion which, by analogy with the quiescent diffusion layer, increases the onset wavelength consistent with the small δ/λ observed in quasisteady state in Fig. 2(a).

In conclusion, our measurements of δ/λ at early times are consistent with theoretical models [4–6] supporting their validity. We have measured both the finger coarsening dynamics and steady-state convective mass transfer and outlined a new stability problem to predict the mass transfer. Our experimental results are useful for understanding the impact of reservoir parameters on the effectiveness of CO_2 sequestration. Permeability K accounts for much of the variability in Ra between different reservoirs. A recent survey of reservoirs in the Alberta basin [20] found a maximum Ra ≈ 1000. Extrapolating our best-fit power law to this lower Ra yields Nu ≈ 10. However, other reservoirs [21] have significantly higher K with Ra $\approx 20\,000$ and Nu ≈ 80. At a reservoir depth of 50 m, the diffusive mixing lifetime of $t_d \approx 16\,000$ yr is reduced by convective processes to approximately 200 yr.

*Corresponding author.
backhaus@lanl.gov

[1] G. Ahlers, S. Grossmann, and D. Lohse, Rev. Mod. Phys. **81**, 503 (2009).
[2] D. Metz, O. Davidson, H. de Connick, M. Loos, and L. Meyer, *IPCC Special Report On Carbon Dioxide Capture and Storage* (Cambridge University Press, New York, 2005), Chap. 5.
[3] T. D. Foster, Phys. Fluids **8**, 1249 (1965).
[4] J. Ennis-King, I. Preston, and L. Paterson, Phys. Fluids **17**, 084107 (2005).
[5] X. Xu, S. Chen, and D. Zhang, Adv. Water Resour. **29**, 397 (2006).
[6] A. Riaz, M. Hesse, H. A. Tchelepi, and F. M. Orr, J. Fluid Mech. **548**, 87 (2006).
[7] J. Ennis-King and L. Paterson, Int. J. Greenhouse Gas Contr. **1**, 86 (2007).
[8] S. Rapaka, S. Chen, R. J. Pawar, P. H. Stauffer, and D. Zhang, J. Fluid Mech. **609**, 285 (2008).
[9] S. Rapaka, R. J. Pawar, P. H. Stauffer, D. Zhang, and S. Chen, J. Fluid Mech. **641**, 227 (2009).
[10] Density and dynamic viscosity data for propylene glycol are taken from manufacturer data, http://dow-answer.custhelp.com/.
[11] A. Hubel, N. Bidault, and B. Hammer, in *Proceedings of the ASME 2002 International Mechanical Engineering Congress and Exposition* (ASME, New York, 2002), pp. 121–122.
[12] T. Kneafsey and K. Pruess, Transp. Porous Media **82**, 123 (2010).
[13] J. A. Neufeld, M. A. Hesse, A. Riaz, M. A. Hallworth, H. A. Tchelepi, and H. E. Huppert, Geophys. Res. Lett. **37**, 22404 (2010).
[14] The shim addenda volume produces a delay in the motion of the interface estimated to be of order of several t^*.
[15] G. S. H. Pau, J. B. Bell, K. Pruess, A. S. Almgren, M. J. Lijewski, and K. Zhang, Adv. Water Resour. **33**, 443 (2010).
[16] The flow is not divergence-free as shown by Eq. (9) in [15]. However, the source term in [15] is only significant within the diffusion interface and is compensated by a vertical adjustment of the water free surface above the diffusive interface.
[17] G. Taylor, Proc. R. Soc. A **219**, 186 (1953).
[18] There are corrections of order 5% due to the small density differences between the fluids.
[19] J. Otero, L. A. Dontcheva, H. Johnston, R. A. Worthing, A. Kurganov, G. Petrova, and C. R. Doering, J. Fluid Mech. **500**, 263 (2004).
[20] H. Hassanzadeh, M. Pooladi-Darvish, and D. Keith, Transp. Porous Media **65**, 193 (2006).
[21] R. Chadwick, D. Noy, R. Arts, and O. Eiken, Energy Procedia **1**, 2103 (2009).